

Ammonia synthesis from N₂ and H₂O using a lithium cycling electrification strategy at atmospheric pressure†

Joshua M. McEnaney,^a Aayush R. Singh,^a Jay A. Schwalbe,^a Jakob Kibsgaard,^b John Lin,^a Matteo Cargnello,^{ab} Thomas F. Jaramillo^{*ab} and Jens K. Nørskov^{*ab}

Ammonia production is imperative to providing food for a growing world population. However, the primary method of synthetic ammonia production, the Haber Bosch process, is resource demanding and unsustainable. Here we report a novel ammonia production strategy, exemplified in an electrochemical lithium cycling process, which provides a pathway to sustainable ammonia synthesis *via* the ability to directly couple to renewable sources of electricity and can facilitate localized production. Whereas traditional aqueous electrochemical approaches are typically dominated by the hydrogen evolution reaction (HER), we are able to circumvent the HER by using a stepwise approach which separates the reduction of N₂ from subsequent protonation to NH₃, thus our synthesis method is predominantly selective for ammonia production. Density functional theory calculations for thermodynamic and diffusion energy barrier insights suggest that Li-based materials are well suited to carry out this process, though other materials may also be useful. The three steps of the demonstrated process are LiOH electrolysis, direct nitridation of Li, and the exothermic release of ammonia from Li₃N, which reproduces the LiOH, completing the cycle. The process uses N₂ and H₂O at atmospheric pressure and reasonable temperatures, and, while approaching industrial level electrolytic current densities, we report an initial current efficiency of 88.5% toward ammonia production.

Broader context

Moving toward sustainability of global scale processes such as ammonia production is a key environmental goal. This work presents an introduction and demonstration of a novel electrochemical cycling strategy with unprecedented current efficiency and selectivity for ammonia production from reagents of only water, nitrogen, and electricity. While conventional ammonia synthesis requires high pressure infrastructure, centralization with distribution, and fossil fuels with high CO₂ emissions, this cycling strategy provides the basis for a sustainable alternative path among limited-to-no options for amenability of renewably powered, potentially localized ammonia production. The demonstrated process is the unique combination of LiOH electrolysis, Li nitridation, and Li₃N hydrolysis, performed in a stepwise cycle to circumvent the hydrogen evolution reaction (HER). Applying this strategy to bypass the HER represents a completely new approach to aqueous-based electrochemical ammonia synthesis which is traditionally dominated by the HER, and this approach may be generally applicable to a variety of systems. Developing electrification and decentralization strategies such as this are important to achieving the long-term goal of process sustainability.

Introduction

The development of a sustainable route to ammonia production is one of the largest challenges in chemistry. The world's ammonia-based fertilizer is predominantly supplied by the industrial Haber–Bosch process and by the enzymatic nitrogenase process.¹ These two

processes are very different. Nitrogenase reduces N₂ molecules at ambient conditions using high energy electrons released through the hydrolysis of 16 ATP molecules.² The Haber Bosch process, on the other hand, uses H₂ molecules with an iron-based catalyst at high temperature (400–500 °C) and high pressure (150–250 bar), conditions which generally require centralized production.³ This process alone produces over 150 million metric tons of ammonia each year and consumes over 1% of the entire global energy supply. Due to the use of hydrocarbon reforming to produce the required hydrogen, it also results in the release of over 450 million metric tons of CO₂ annually.⁴ It would be desirable to develop an alternative, sustainable process capable of employing renewable resources rather than fossil fuels to produce fertilizer locally where it is used. To this end,

^a SUNCAT Center for Interface Science and Catalysis, Department of Chemical Engineering Stanford University, Shriram Center, 443 Via Ortega, Stanford, CA 94305, USA. E-mail: jaramillo@stanford.edu, norskov@stanford.edu

^b SUNCAT Center for Interface Science and Catalysis, SLAC National Accelerator Laboratory, 2575 Sand Hill Road, Menlo Park, CA 94025, USA

† Electronic supplementary information (ESI) available. See DOI: 10.1039/c7ee01126a

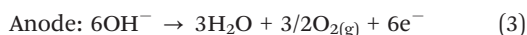
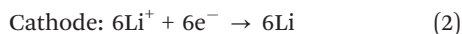
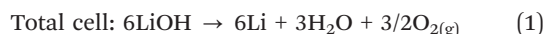
attempts have been made to mimic the enzymatic process with molecular complexes, achieving high selectivity under strongly reducing conditions, however the stability of these catalysts is a challenge.^{5,6} Many photochemical and electrochemical routes to ammonia from N_2 and H_2O using heterogeneous catalysts have been explored.^{7–11} NH_3 production and current efficiencies are usually below 1% due to the exceptional stability of the N_2 triple bond and due to competition with the hydrogen evolution reaction (HER). Experimentally, some progress has been made by moving to molten salt systems, which have allowed for higher selectivity of ammonia over hydrogen evolution.^{12,13} Fundamentally, however, it remains a challenge to provide protons and electrons at high enough chemical potential to reduce nitrogen without producing substantial amounts of H_2 .

In this work, we outline and demonstrate an alternative strategy, which physically and temporally separates the reduction of N_2 from the subsequent protonation to ammonia, thus circumventing the HER. Essentially, voltage is applied to produce a highly reactive surface in a proton-free environment. This surface is then exposed to nitrogen, activating it to produce a nitride phase. The voltage is then released and protons are added to yield ammonia. We realized this concept experimentally in a complete electrolytic and chemical reaction cycle using lithium metal as the reactive species. Lithium was chosen for its well-understood electrochemistry and ability to activate nitrogen at ambient conditions. The demonstrated cycle comprises the unique combination of LiOH electrolysis, Li nitridation, and Li_3N hydrolysis to produce ammonia. Each step in the overall process yielded significant scientific advancements as LiOH electrolysis was designed to perform with high efficiency, we provide the first fundamental understanding of why the nitridation of Li is facile which is broadly applicable to the ability of a metal to activate N_2 , and we have developed a succinct quantification and verification strategy for proving N_2 is the source to form NH_3 . We report a current efficiency of 88.5% for ammonia production *via* this process.

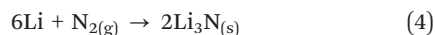
Results and discussion

The cyclic process is outlined conceptually in Fig. 1. Unlike traditional thermal catalysis or thermochemical looping strategies,^{14,15} this process can be run at ambient pressure, moderate temperature, and requires no H_2 . It can be powered sustainably by using solar or wind resources to provide the necessary electric energy. The figure shows the three steps:

Step 1: LiOH electrolysis:



Step 2: Direct reaction of metallic Li with N_2 to form Li_3N :



Step 3: Release of NH_3 by reaction with H_2O :

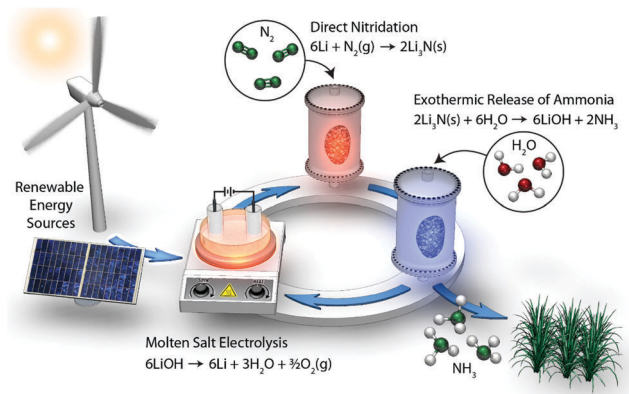


Fig. 1 Sustainable ammonia synthesis concept cycle.

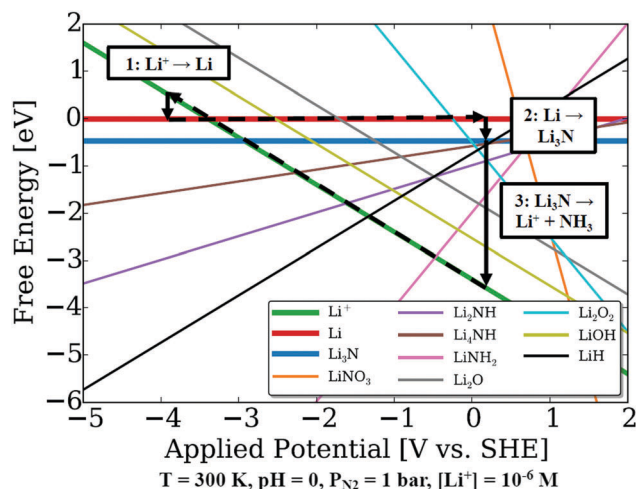


Fig. 2 Phase diagram showing the relative thermodynamic behavior of Li-N-O-H species with the proposed Li cycle steps superimposed.

The fundamental principles governing this process are illustrated in the Li-N-O-H phase diagram shown in Fig. 2. At an electric potential U and temperature T , the Gibbs free energy (or the total chemical potential), $\Delta G_i(U, T)$, for each species i , relative to metallic Li, gaseous N_2 , liquid H_2O (a reasonable oxygen reference because it is the most likely experimental source of oxygen in the system), and gaseous H_2 , is given by the following expression for $Li_wN_xO_yH_z$:

$$\begin{aligned} \Delta G_i(U, T) = & \Delta H_i^0(T) - T\Delta S_i^0(T) - y_i\Delta G_{H_2O}^0(T) \\ & + (w_i - 1) \Delta G_{Li/Li^+}^0(T) - k_b T \ln([Li^+]) \\ & - \frac{1}{2}x_i k_b T \ln(P_{N_2}) - (2y_i - z_i)k_b T(\text{pH}) \\ & + (w_i - 1 - 2y_i + z_i)eU \end{aligned}$$

Here, $\Delta H_i^0(T)$ is the standard heat of formation obtained from the Materials project database^{16,17} and $\Delta S_i^0(T)$ is the standard entropy change associated with the removal of gas phase species. $\Delta G_{H_2O}^0$ and $\Delta G_{Li/Li^+}^0$ are the standard Gibbs free energies of formation of liquid H_2O (from gaseous H_2 and O_2) and metallic

Li (from Li^+ and an e^-), respectively. $[\text{Li}^+]$ and P_{N_2} are the Li^+ ion concentration and gaseous N_2 pressure relative to standard state.

Fig. 2 outlines the three steps in the proposed cycle superimposed on a phase diagram of the relevant solid lithium surface species. It is important to note that this phase diagram is created under a specific set of conditions: at a temperature of 300 K, a pH of 0, a Li^+ ion concentration of 10^{-6} M, and all reference pressures of 1 bar. All of these conditions are variables that can be adjusted freely from step to step to obtain the best possible experimental performance, but because the energy differences in the diagram are substantial (for the most part greater than 1 eV), the physical picture remains largely the same over a wide range of parameter space. The stepwise process provides the advantage of specifically avoiding selectivity issues which can be identified in the phase diagram. The features that we exploit are as follows: first, in Step 1, we start with lithium ions with no protons or nitrogen available. Under the aqueous theoretical conditions shown, Li^+ ions can be reduced to Li metal at potentials more negative than -3.3 V *vs.* the standard hydrogen electrode (SHE). LiH and other hydrogen containing phases are shown to be thermodynamic sinks in this system, however, when Step 1 proceeds in the absence of protons, both hydrogen evolution and the formation of these phases are mitigated. Next, lithium nitride is shown to be more stable than lithium under all given potentials at 1 bar of nitrogen gas pressure, a feature exploited in Step 2, in which nitrogen is added to the lithium in an aprotic environment to form the nitride. Fortunately, this reaction is not only energetically favorable, but also kinetically fast, which allows it to proceed at mild temperatures.¹⁸ Finally, protons are introduced to the lithium nitride at 0 V *versus* SHE in Step 3. At this potential, the lithium nitride rapidly and spontaneously breaks down to ammonia and lithium ions, completing the cycle.

We have experimentally demonstrated the proposed electrothermochemical cycling process. First, LiOH is electrolytically reduced to Li. Similar processes are standard in *e.g.* Li ion batteries. We chose to illustrate the electrolysis in a LiCl-KCl/LiOH-LiCl controlled molten salt mixture (Step 1). While molten salt electrolysis can generally allow for effective isolation of unreacted Li metal product, efficient molten LiOH electrolysis is challenging and rare in the literature due to the material-limiting conditions of using a molten strong base and due to potential side reactions and reverse reactions with metallic Li.^{19,20} We designed our molten electrolysis cell to include a porous alumina diffusion barrier around the counter electrode (and LiOH-LiCl) to mitigate the reaction of LiOH, H_2O , or O_2 with the Li product at the working electrode (Fig. 3A). Consequentially, the formation of thermodynamic sinks, such as LiH, can be minimized. The melt was held at 450 °C to ensure a continuous liquid phase was maintained throughout the electrolysis process, though lower temperatures are possible in a refined system or with lower melting point salt mixtures. The general electrochemical behavior of this cell was evaluated using cyclic voltammetry, testing the cathode and the anode individually as working electrodes between -0.9 V and 3.9 V *versus* Li/Li⁺, as shown in Fig. 3B. These experiments indicated a total cell potential minimum of ~ 3.0 V for LiOH

electrolysis at 450 °C. This is comparable to the theoretical required potential of 2.8 V at 700 K (427 °C), based on an estimation of Gibbs energy referenced from the JANAF thermochemical tables.²¹ Similar minimum potentials and temperatures (3.6 V at 427 °C) are required for standard industrial Li metal production *via* LiCl electrolysis in a LiCl-KCl molten bath.²² Current efficiency toward lithium production from LiOH electrolysis was evaluated by synthesizing lithium using 200 °C of charge from specific applied currents as shown in Fig. 3C. The average current efficiency to Li product over the three distinct experiments was 88.5% (S.D. = 0.8%).

To demonstrate cell stability and cyclability, consecutive electrolysis experiments were performed at 0.7 A for 3000, 3000, and 6000 seconds and at 1.5 A for 1500 seconds with excess LiOH added in-between each run (see ESI,† Fig. S1). As H_2O and O_2 were evolved at the anode, the built-in glove box detection of these species increased, indicative of LiOH electrolysis. To test for the possible formation of Cl_2 gas, potassium iodine starch paper was exposed throughout testing which was consistently negative for the formation of Cl_2 gas under electrolytic conditions. This is consistent with prior literature results.^{19,20} Additionally, potassium species from possible KCl electrolysis were not observed in cross-sectional X-ray photoelectron spectroscopy (XPS) of the Li products, even at high applied potentials (Fig. S2, ESI†).

For chemical conversion of Li to Li_3N (Step 2), electrolytically synthesized Li samples were exposed to a flowing N_2 atmosphere and held at temperatures between 22 and 100 °C. We tested the conversion efficiency of Li to NH_3 by adding the Li_3N to H_2O , which rapidly hydrolyzed the nitride to yield ammonia (Step 3). As indicated by Fig. 3D, initial conversion rates to Li_3N can be increased by increasing temperature. Overnight flow (12 h) resulted in a near complete conversion to the nitride regardless of applied temperature (22, 50, and 100 °C) as indicated by the approximately 100% conversion efficiencies to NH_3 in Fig. 3D. Notably, complete conversion would therefore result in approx. 100% selectivity to NH_3 from Li used. The X-ray diffraction (XRD) pattern in Fig. 3E shows that the Li was successfully converted to Li_3N . Trace amounts of LiOH and Li_2O also appear in the diffractogram, arising during Li transfer from the electrochemical cell to the N_2 tube furnace, where the sample is exposed to O_2 and H_2O from ambient air. This is consistent with findings from previous reports, which also indicate that increased nitridation rates can be expected as a result of H_2O and O_2 exposure.^{18,23,24} To complete the Li cycle, LiOH recovery was evaluated by evaporating H_2O and NH_3 at 120 °C. Anhydrous LiOH was isolated and recovered, as shown by the XRD data in Fig. 3E, with an efficiency of 98% *vs.* the initial amount of Li used in Step 2. By adding LiOH periodically back into our cell, we establish the cycling concept of this complete ammonia synthesis process.

In order to reliably detect and quantify ammonia, we employed two complementary methods: a modified version of the indophenol colorimetric test and Fourier transform infrared spectroscopy (FTIR). The indophenol test (Berthelot's reaction), its salicylate analog, and Nessler's reagent have been used

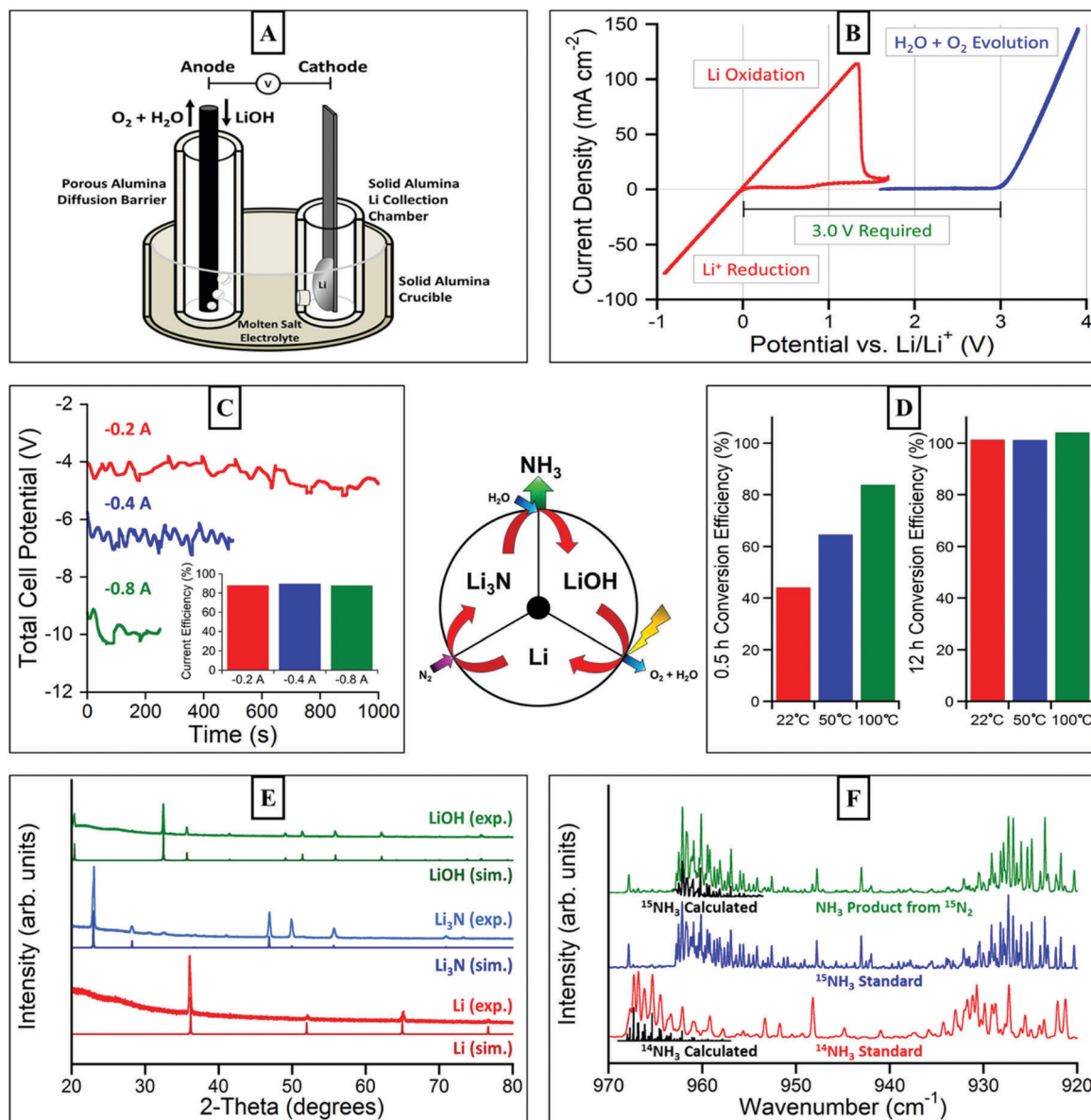


Fig. 3 Experimental characterization. (A) Schematic cross-section of the electrolysis cell. (B) Cyclic voltammetry showing potential sweeps of the steel working electrode cathode electrochemical cell between -0.9 V to 1.7 V vs. Li/Li^+ at 450 °C, and of a Pt working electrode anode between 1.6 V and 3.9 V under the same conditions. (C) Electrochemical galvanostatic LiOH electrolysis with corresponding (inset) current efficiencies toward lithium yield. (D) Ammonia yield from Li nitridation under different conditions to Li_3N then reaction with H_2O . (E) XRD data for experimentally synthesized (exp.) and simulated (sim.) Li intermediate products (F) FTIR spectra for isotopically labeled ammonia indicative of synthesis from $^{15}\text{N}_2$.

in many reports of ammonia synthesis.^{7,25–27} While ammonia can be readily quantified to sub-ppm levels with UV-Vis spectroscopy (Fig. S3, ESI[†]), such colorimetric tests are susceptible to interferences and false positives from other sources of reduced nitrogen, such as chloramines found in tap water, contaminants in Nafion[®] and other membranes, and amines found in epoxies.²⁸ This technique was therefore complimented by FTIR spectroscopy, which offers a more specific ammonia signal for verification and the opportunity to perform isotopically labelled studies. Both techniques were calibrated with stock solutions of ammonium hydroxide and optimized for consistency and sensitivity.

To examine whether the ammonia we detect comes from the gaseous N_2 inlet or from an unexpected, adventitious nitrogen source, isotopically labelled studies were performed. The ammonia synthesis procedure was identical to that used in other experiments, except that $^{15}\text{N}_2$ was used in place of the dominant natural isotope, $^{14}\text{N}_2$. By means of FTIR, we unambiguously identified the presence of labelled ammonia ($^{15}\text{NH}_3$) vs. that of the natural isotope ($^{14}\text{NH}_3$). As shown in Fig. 3F, the FTIR spectrum of ammonia produced in the cycling experiment matches the $^{15}\text{NH}_3$ peaks from the ^{15}N labelled ammonia standard. These spectra are also in good agreement with the predictions of the quantum harmonic oscillator and the

HITRAN database.²⁹ Given the extremely low natural abundance of ¹⁵N, the labeling experiments prove that the ammonia produced in the cycling process indeed comes from the gaseous N₂ inlet and not from direct or indirect contamination.

There are two key aspects which motivated the choice of Li as the reactive species, the fact that N₂ dissociates spontaneously over metallic Li^{23,30,31} and the ease of diffusion processes associated with the room temperature formation of bulk Li₃N. We used density functional theory (DFT) calculations (see Experimental section for calculation details), to further analyze

these two properties. The ease of dissociation of the strong N–N bond is particularly interesting, given how difficult this process is for transition metals.^{32–35} Our calculations do indeed show small barriers for N₂ activation on various sites of the Li BCC (110) facet under multiple nitrogen coverages (Fig. 4A inset). Interestingly, the barrier follows the scaling relation between barrier height and N–surface bond strength found for the transition metal surfaces used in the Haber Bosch process (Fig. 4A). Li is only special, in regards to N₂ dissociation, for having a very strong bond to atomic N. Therefore, other simple

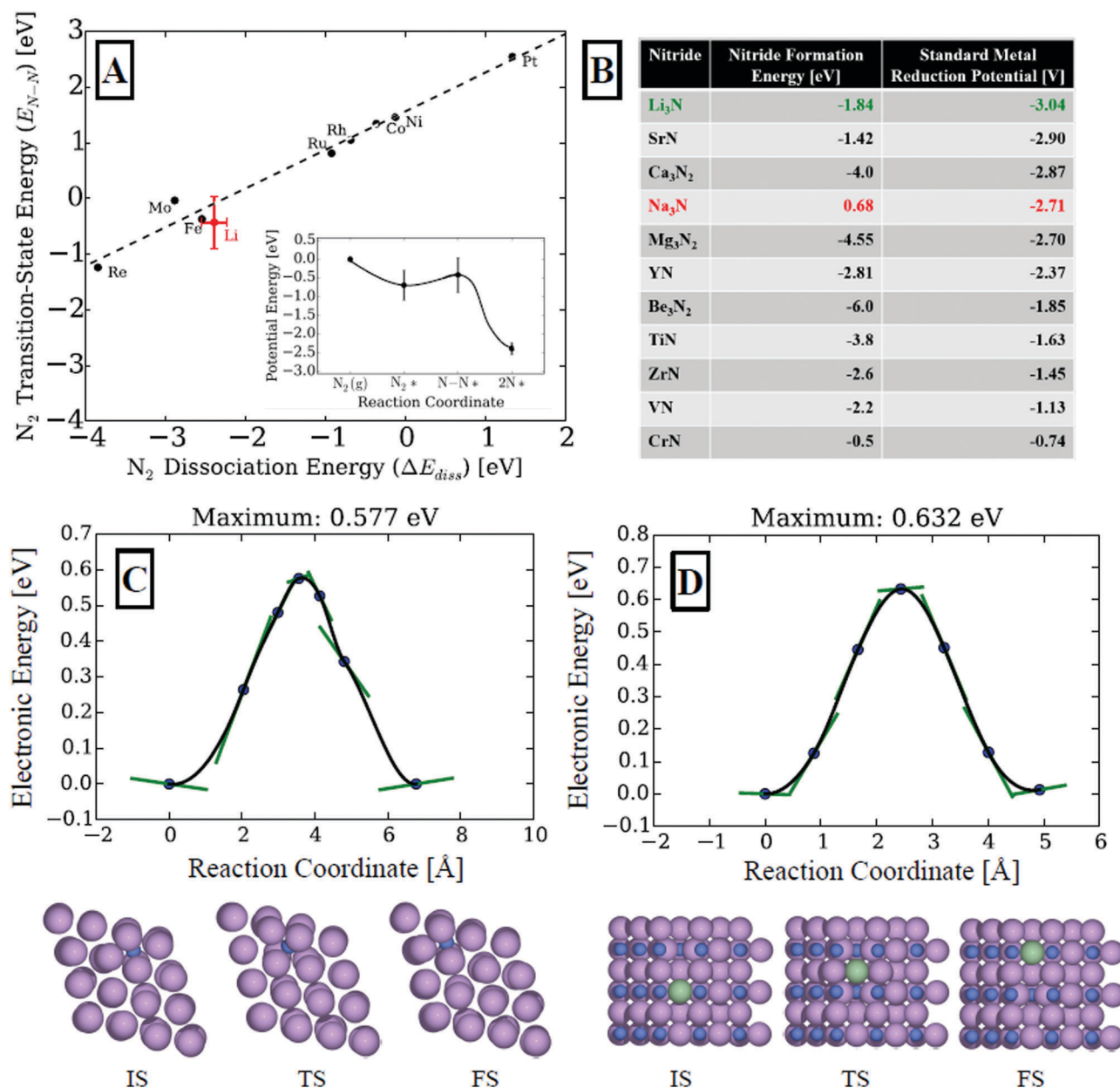


Fig. 4 Theoretical analysis. (A) Scaling relationship between the energies of N₂ dissociation and the N–N transition state energies on stepped transition metal surfaces (black) with the Li BCC (110) facet overlaid in red. The energy profile for N₂ dissociation on Li is also shown (inset). (B) Table comparing metal nitride cycle candidates. (C and D) Diffusion energy barriers of bulk Li₃N formation, modeling nitrogen (blue) diffusion in a bulk Li (purple) body-centered-cubic lattice (C) and modeling diffusion of a chosen Li atom (green) in a bulk Li₃N lattice (D). The green lines in the graphs represent the converged forces on the images, mostly along the reaction coordinate.

metals with a strong bond to N are also candidates for the conceptual approach introduced in this work.

To investigate the possibility of using metals other than Li we compare in Fig. 4B the nitride formation energies and electrochemical reduction potentials for various metals. An ideal material would form from ions requiring a relatively low applied potential, yet form a stable nitride, and possibly offer a more favorable nitrogen stoichiometry compared to the 3:1 ratio of Li_3N . Considering these criteria, promising candidates include Zr, V, Cr, and Ti amongst others for nitridation. Kinetic parameters such as atomic size and mobility may also play a role in the successful cycle demonstrated here with lithium; other metal nitrides might not necessarily form as easily under ambient conditions, even with favorable formation energies. While unique experimental challenges might affect any alternative metal cycles, this analysis indicates that other cycles might indeed still be feasible.

For the bulk diffusion processes, we investigated both nitrogen diffusion in a bulk Li BCC lattice (Fig. 4C) and lithium diffusion in Li_3N (Fig. 4D). In Fig. 4C and D, nudged elastic band transition state (TS) calculations were used to evaluate electronic energy relative to the initial state (IS) as a function of the reaction coordinate (total atomic movement across the pathway projected onto a one-dimensional distance). In both subfigures, the position of the diffusing atom in the initial and final states (FS) is the most stable location of that atom in the unit cell, as determined by multiple DFT relaxations. Our calculations indicate that the processes have activation barriers of approx. 0.6 eV, which is readily surmountable at room temperature. One reason for the facile nitridation of lithium may be that the lattice structures of Li and Li_3N are particularly flexible. As seen in the structures shown in Fig. 4C and D, the bulk structures of the lattices are able to deform readily as the N or Li atom moves, resulting in a lower energy transition state for diffusion than would likely exist for a more rigid material. Lattice flexibility, measured indirectly by the diffusion barrier or more directly by materials properties such as the bulk modulus, may also help to narrow the list of possible materials that are suited for the cyclic process discussed here.

The ammonia synthesis strategy outlined and demonstrated in this work offers a number of particular advantages over conventional Haber Bosch ammonia synthesis: Operation at ambient pressure, the use of water instead of H_2 , and the possibility of direct coupling to renewable sources of electricity (e.g. wind, solar), all of which promote amenability for local, on-site production. These attributes make it a complementary process to Haber Bosch with potential near-term applications in new sectors and markets. De-centralized production of ammonia fertilizer could be beneficial in a number of ways: the distribution costs would be substantially reduced and nitrogen utilization efficiencies could be significantly improved (currently approx. 50% globally based on crop uptake) by enabling continuous application, possibly coupled to irrigation systems during crop growth rather than bulk application with wasteful runoff.³⁶ On-site production is the best way to realize these benefits. While stored tanks of anhydrous ammonia from

conventional production could also be used to integrate with precision agriculture, storing concentrated anhydrous ammonia at the point of use would have regulatory hurdles, distribution costs, and safety concerns as disadvantages. In addition to increasing efficiency in modern agriculture, farming in the developing world could be facilitated greatly, particularly in locations where there is minimal infrastructure for the distribution of centralized fertilizer. Importantly, the ability to use H_2O rather than H_2 as a hydrogen source could also readily decouple ammonia production from fossil resources, which would not only reduce susceptibility to regional and temporal fluctuations in cost and supply, but also have an impact on CO_2 emissions as currently, ammonia production accounts for approx. 1% of all global CO_2 emissions.⁴ Another method to mitigate CO_2 is to use water electrolysis to make H_2 which is a promising strategy that is currently being explored.³⁷ The hydrogen is then used as a reactant feed for conventional NH_3 synthesis, thus the high pressure infrastructure requirement remains and the water electrolysis method is therefore not highly amenable to significant decentralization and related advantages at this point, which contributes to the importance of exploring new strategies.

Whereas in the Haber Bosch process the dominant costs arise from producing H_2 from fossil fuels and from the high pressure reaction that require high capital and operational expenditures, for the electrochemical process described herein the dominant costs are expected to involve the electricity required to reduce Li^+ to Li.^{38,39} While this is a laboratory-scale demonstration, and other factors such as air separation to acquire N_2 , product separations, and higher voltages may impact total energy cost, the minimum required process energy cost from the LiOH electrolysis at 3 V amounts to ~ 14 kW h per kg NH_3 (see Experimental section for further details). This is a highly favorable result as the overall conventional process average energy cost is ~ 10 kW h per kg NH_3 , and coal powered ammonia plants in China require an average of ~ 15 kW h per kg which indicates that this potentially sustainable and decentralized process is remarkably near the region of the Haber Bosch energy cost.⁴ Further energy cost analysis will require specific details of device scale, features, and desired output. However, we do note that this process may not require ultra-pure nitrogen as some Li_2O from O_2 contamination would also reform LiOH during hydrolysis and allow the cycle to continue, whereas O_2 contamination is detrimental to catalytic performance in typical Haber Bosch catalysis.³⁸ Despite the high reduction potential characteristic of the electrolysis reaction, a preliminary analysis indicates that at low electricity prices, electricity costs from electrolysis are reasonable for the production of ammonia by this method (see Experimental section and Fig. S4, ESI† for details). Thus, an efficient process performed at expected cell potentials near 4 V as demonstrated in this work, is promising for complementary ammonia synthesis driven by potential sustainability of the process, low cost of renewable electricity, subsidies to decrease CO_2 emissions, increased nitrogen utilization efficiency potential for lower required ammonia fertilizer, localized production with lower cost

infrastructure, or some combination of these possible advantages. Notably, the wholesale costs of wind and solar electricity have been decreasing substantially over time and are projected to become the cheapest sources of electricity for many regions and most countries in the years to come, highlighting the importance of developing scientific routes to the electrification of major chemical processes, particularly those involving a large carbon footprint, such as ammonia synthesis as discussed in this work.⁴⁰

Conclusions

In summary, we have developed a novel electrochemical ammonia production strategy, exemplified by a lithium-mediated cycling process for synthesizing ammonia from N_2 and H_2O at ambient pressures. By design, this electrochemical cycling strategy is capable of exceptional efficiency and selectivity compared to typical aqueous electrochemical approaches due to the ability to circumvent the otherwise competing and dominant hydrogen evolution reaction. The demonstrated process has an initial overall current efficiency of 88.5% to ammonia, based on the individually determined efficiencies of each step in the synthesis. Importantly, isotopic labeling studies with $^{15}\text{N}_2$ conclusively showed that N_2 was the nitrogen source for the ammonia produced by this process. Theoretical analysis suggests that, based on this generalized strategy, other metal systems may continue to improve upon the metrics of efficient electrochemical ammonia production, opening up a new avenue of research to explore. While we have depicted a step-wise reaction scheme to effectively introduce and demonstrate the lithium reaction cycle, a continuous process in a compartmentalized device would be beneficial for implementation. Initial techno-economic electricity cost analysis and energy input considerations for this process reveal promise for suitable markets, especially considering the advantages of this process which can use renewable resources, mitigate CO_2 emissions, and be readily de-centralized compared to conventional, centralized ammonia synthesis.

Experimental

Chemicals and materials

Lithium hydroxide [$\geq 98\%$, LiOH, powder, Sigma-Aldrich], lithium chloride [$\geq 99\%$, LiCl, anhydrous powder, Sigma-Aldrich], potassium chloride [$\geq 99\%$, KCl, anhydrous powder, Sigma-Aldrich], stainless steel foil [Fe:Cr:Ni; 70:19:11 wt%, 0.5 mm thick, Alfa Aesar], graphite rod, nickel rod, lithium ribbon [99.9%, 1.5 mm thickness, Sigma-Aldrich], nitrogen gas [ultra high purity, 99.999%, Praxair], $^{15}\text{N}_2$ gas [98%+, Cambridge Isotope Lab], $^{15}\text{NH}_3$ gas [98%, Cambridge Isotope Lab], STI ammonia test kit, DI Millipore water, porous alumina diffusion barrier tube [80 mm height \times 27 mm outer diameter (OD) \times 3 mm thickness, P-3-C material, 1.7 μm average pore diameter, single closed end tube, Coorstek], alumina round dish [35 mL, 25 mm height \times 50 mm OD \times 3 mm thick,

AdValue Technology], cylindrical alumina crucible [5 mL, 26 mm height \times 20 mm OD \times 1 mm thick, 2 mm diameter side wall hole, AdValue Technology].

Electrolysis of LiOH

Reactions were performed in an electrochemical cell made of chemically resistant aluminum oxide which was encased in high-temperature, insulated heating tape or heating mantle with a thermocouple to maintain temperature. The cell was equipped with a porous alumina cylindrical diffusion barrier to effectively isolate anodic and cathodic reactants and products and prevent undesirable side reactions. The cell apparatus is outlined in Fig. 3A in the Results and discussion section. Typically, a steel cathode and graphite rod anode were used for electrolysis reactions, though other materials (Ni, W, Ti, Pt) could be used as well. We note that nickel and graphite anode materials may not be suitable for long term cycling as some corrosion was observed under working conditions in the molten hydroxide. All reactions were held between 400–450 °C. Molten Li product was collected in a solid alumina cylindrical crucible, surrounding the steel working electrode, with a 2 mm hole bored into the bottom of the side wall to allow for molten salt flow and conductivity. Prior to electrochemical testing, a 30 s hold with a total cell voltage of -2 V was applied to purge the system of residual H_2O . For cyclic voltammetry studies, a steel working electrode and Pt pseudo reference electrode were used and voltage was applied between -0.9 V to 1.7 V vs. the Li/Li⁺ zero reference point. Pt was used as the anode, also measured as a working electrode, with an applied voltage between 1.6 V and 3.9 V vs. Li/Li⁺. For Li electrolysis, a constant current (0.2–2.0 A) was applied, approaching that of industrial electrolyzers, with potential recorded over time.

To determine relative current efficiencies at different approximate potentials, three experiments of theoretically equivalent Li production were performed. Currents were applied at 0.2 A for 1000 s, 0.4 A for 500 s, and 0.8 A for 250 s (200 °C each) resulting in a theoretical yield of 0.01439 g Li based on Faraday's laws of electrolysis. As molten Li cooled on the steel electrode, segregated salts also crystallized making direct mass yield challenging. Instead, Li product was controllably released under water and hydrogen gas evolved which was collected *via* controlled gas displacement. NOTE: lithium reacts violently with water, thus only appropriately trained personnel with proper safety precautions and PPE should attempt these reactions. Using purchased Li metal as controls and the ideal gas law, Li yield was calculated giving the current efficiency for each reaction. The amount of molten Li formed under these conditions remained attached to the steel electrode after electrolysis, whereas excess Li from longer electrolysis reactions forms distinct floating, molten Li pools above the molten salt.

Li₃N synthesis from Li and N₂

Li was produced in excess from LiOH electrolysis and collected from the small crucible containing the steel working electrode and the molten salt mixture. The melt was transferred to a steel crucible and allowed to cool. Li metal was brought above its

melting temperature (180 °C) to isolate it from molten salt impurities, and the liquid product was decanted into a second steel crucible. Solid, cooled Li was cut and pressed between steel into a ~ 1 mm thick pellets. The mass of these Li pellets was measured (approx. 0.1 g each) and the pellets were transferred from the Ar glovebox in a septum capped vial to a N_2 purged tube furnace. Li was very briefly (15 s) exposed to air where the surface would slightly tarnish during transfer. A slight presence of O_2 and/or H_2O is believed to improve nitrogen uptake by Li metal according to literature reports, whereas very pure N_2 will react more slowly with Li if at all at room temperature.^{18,23} Li was heated to 22–100 °C in the N_2 atmosphere for 0.5–12 h. This procedure was identical for $^{15}N_2$ FTIR control studies (100 °C for 12 h). Under these conditions, we estimate a rate range of 1–3% Li converted per min depending on the temperature applied, which may be improved further with thinner films, higher temperature, or increased N_2 pressure for larger scale application. We also note that in an eventual continuous operation device (conceptualized, for example, in ESI,† Fig. S5) the separation and pressing of the Li could be significantly simplified or unnecessary.

Ammonia synthesis from Li_3N and H_2O

Li_3N pellets were removed from the N_2 atmosphere tube furnace and placed into a scintillation vials containing 10 mL Millipore purified, de-ionized H_2O . Caution: If conditions are not optimized, poor Li to Li_3N conversions are possible, therefore significantly more H_2O should be used with a larger headspace container as Li reacts violently with H_2O to release minimally soluble H_2 gas, whereas Li_3N with H_2O results in a rapid but non-violent reaction, producing water-soluble ammonia.

Ammonia detection and quantification

Ammonia was detected *via* two spectroscopic methods: colorimetric ultra violet-visible light (UV-Vis) spectroscopy and Fourier transform infrared radiation (FTIR) spectroscopy. A colorimetric indicator method was coupled with UV-Vis spectroscopy for precise quantification from an ammonia standard calibration curve (Fig. S3, ESI†). The colorimetric method first uses a solution of dilute hypochlorous acid, from the STI ammonia detection kit, to convert NH_3 to NH_2Cl . Chloramine then reacts with a second solution containing dilute salicylate ions (yellow) to form 5-aminosalicylate, which can oxidatively couple with a second salicylate molecule to yield a blue compound known as indophenol (4-(4-hydroxyphenyl)-iminocyclohexa-2,5-dien-1-one). The combination of the yellow and blue colored molecules appears green, observed as a scalable hue from yellow to blue with increasing ammonia concentration. Samples were carefully diluted and tested to obtain accurate ammonia yields from Li_3N reaction. As the synthesized Li_3N typically contained trace impurities from brief reaction with air, we calculated ammonia yields based on the theoretical yield from the mass of Li used. FTIR detection provides a clear and specific signal for NH_3 synthesis verification. To get the highest quality spectra, we used gas phase FTIR,

rather than liquid phase. To accomplish this, a small (200 μ L) sample of a synthesized NH_3 solution was then fully vaporized into a 2 m gas cell, mounted in a Nicolet spectrometer using a homebuilt volatilizer. To minimize ammonia lost in the apparatus, all surfaces were heated to at least 120 °C and the total surface area that the sample saw was minimized. Ammonia standards made from ammonium hydroxide and isotopically labeled ammonia were used to calibrate and test the detector.

Recovery of LiOH and cycle completion

The reaction between Li_3N and H_2O reproduces LiOH, completing the ammonia cycle. LiOH was dried and re-introduced to continue the cycle with production of Li metal. To test the initial Li cycle efficiency, LiOH yield was determined by converting a known amount of Li to Li_3N and then to LiOH in water, and evaporating the water in a boat within a N_2 atmosphere tube furnace at 120 °C for 3 h to dryness. LiOH powder was then characterized by XRD and its mass was taken to compare *vs.* the theoretical yield from Li mass.

Preliminary techno-economic considerations and electricity calculations

We note that many factors including design, scale, and speed of production will effect costs, and thus a more in-depth study will be required to give a complete picture, however assuming that electricity of the electrolysis is the primary expense, ESI,† Fig. S4 outlines the cost of electricity toward ammonia synthesis *via* this method with respect to recent United States Department of Agriculture price data for ammonia, indicating than an efficient process driven at expected cell potentials near 4 V, as demonstrated in this work, is promising for complementary ammonia synthesis.⁴¹ Fig. S4 (ESI†) considers cost at $\$0.071$ kW h⁻¹, the industrial average for electricity cost, at $\$0.02$ kW h⁻¹, the levelized cost of inexpensive hydroelectric power, and at $\$0.01$ kW h⁻¹, an optimistic electricity cost from intermittent over-production, low-demand electricity or a possible long-term regional renewable electricity cost if trends continue, indicating overall that cheaper than average electricity will be highly preferable for this process.^{40,42} The cost of maintaining molten salt reaction temperatures is expected to be comparably low as evidenced by advances in molten salt energy storage technologies with high temperature maintenance efficiencies as well as by intrinsic heating from electrochemical resistance of industrial, insulated molten salt electrolysis.^{43–45}

For electricity cost calculations to produce one metric ton of NH_3 , we calculated the effective number of grams of Li to be cycled which corresponds to a number of coulombs of electricity required *via* Faradays laws of electrolysis. Then, considering the possible applied potentials, the required joules of energy and thus kiloWatt hours (kW h) could be determined. Factoring in efficiency of electrolysis and cost of electricity per kW h the applied potential could then be correlated to a determined electricity cost toward the production of one metric ton of ammonia (Fig. S4, ESI†). If Li were produced with 100% current efficiency, a minimum power energy cost (reported as

kW h per kg NH₃) can also be determined using a minimum voltage of 3 V at 450 °C.

We explore how reasonable Li metal cost and usage would be considering that, stoichiometrically, 1.22 metric tons of Li need to be cycled to produce 1 metric ton of NH₃. The average farm in the United States according to the USDA (2012) is 434 acres, requiring ~0.077 metric tons of ammonia per acre annually based on nitrogen weight in the applied fertilizer, or 33.47 metric tons NH₃ per farm.⁴¹ Therefore, for the average farm, ~41 metric tons of Li need to be cycled to fulfill the farms annual ammonia requirement, based on this estimate. Thus, if a device used 1 kg of Li, the device would need to cycle that Li 41 000 a year, for 10 kg of Li, 4100 cycles per year, for 100 kg of Li, 410 cycles per year, *etc.* For reference, 10 kg of Li metal is comparable to the amount of Li metal in an electric car battery.⁴⁶ While pure Li metal is somewhat more expensive and less practical to transport, LiOH may be purchased for this process at low cost, currently only ~\$20–30 per kg LiOH, (10 kg Li metal equates to ~34.5 kg LiOH), representing a small initial Li investment for the cycle.⁴⁷

For perspective on possible nitrogen feed separation and use, the average farm would require ~28 metric tons of N₂ based on the calculations above to produce their annual NH₃ requirement. As an example, a Nitroswing[®] commercial pressure swing absorption unit (NS-10) can produce up to ~13.9 kg h⁻¹ N₂, at 99.99% purity, requiring ~1584 h to achieve the annual N₂ requirement, running at 7.5 bar with maximum power consumption of 0.3 kW.⁴⁸ This equates to an energy requirement of only ~0.02 kW h per kg NH₃ toward the nitrogen feed purification step in this example. Lower purity requirements can achieve higher feed production rates. Considering practicality of nitridation rates, literature results indicate that rates can vary widely based on conditions (approx. ~20–130 mmol N₂ uptake per h for ~0.5–5 g Li sample over the first hour). More importantly, complete nitridation has been achieved on a minutes rather than hours or longer time-scale with increased temperature and surface area of Li, which indicates that reasonable rates are attainable for application *via* appropriate design engineering.⁴⁹

Physical characterization

X-ray diffraction (XRD) was performed using a Philips PANalytical X'Pert Pro in parallel beam mode with Cu K α radiation and 0.04 rad Soller slits. Prior to XRD scanning, samples were pressed flat and sealed with Kapton[®] (polyimide) tape against a glass slide backing in an Ar filled glove box. Fourier transform infrared radiation (FTIR) spectroscopy was performed using a Nicolet IS-50 FTIR Advanced Spectrometer equipped with a Nicolet 2 m gas cell (ZnSe windows) connected to heated vapor and vacuum gas lines. Ultraviolet-visible (UV-Vis) spectroscopy was performed using an Agilent Cary 6000i UV/Vis/NIR Spectrometer in absorbance mode across 1 cm path length cuvettes, measured between wavelengths of 400 to 800 nm. X-ray photoelectron spectroscopy (XPS) was performed using a PHI VersaProbe XPS Microprobe with binding energies referenced to adventitious carbon at 284.8 eV. XRD, UV-Vis, and XPS

characterization were performed at the Stanford Nano Shared Facilities (SNSF).

Calculation details for N₂ activation on metallic Li and diffusion barrier for Li₃N formation

All density functional theory (DFT) relaxations and transition-state calculations were performed using the Quantum Espresso software package,⁵⁰ as implemented in the Atomic Simulation Environment (ASE).⁵¹ The BEEF-vdW exchange–correlational functional was used in order to achieve high accuracy in bulk and surface energetics, taking van der Waals interactions into account.⁵² Atoms were allowed to relax until the force on each atom was less than 0.05 eV per atom, using a plane wave cutoff of 500 eV and a density wave cutoff of 5000 eV. All atoms were allowed to relax in bulk calculations, while in surface relaxations the lowest two layers were held fixed to simulate the rigidity of the bulk. A (4 × 4 × 4) bulk unit cell was used for metallic lithium, and a (3 × 3 × 3) alpha-Li₃N bulk unit cell was used for lithium nitride. For surface calculations on metallic lithium, a (4 × 4 × 4) unit cell with 10 Å of vacuum in the z-direction was used. (4 × 4 × 4) and (4 × 4 × 1) Monkhorst–Pack *k*-point grids were used for bulk and surface calculations, respectively.

Authorship contributions

J. M. M. and J. K. N. conceived the study; J. M. M. designed and performed the experiments and coordinated the study; J. M. M. and J. A. S. performed preliminary electrochemical experiments and developed characterization of the products, A. R. S. and J. L. developed and incorporated theoretical contributions; J. K., M. C., T. F. J., and J. K. N. provided mentorship and conceptual advice; all authors contributed to writing the manuscript.

Acknowledgements

This work was supported by Villum Fonden. Part of this work was performed at the Stanford Nano Shared Facilities.

References

- 1 W. E. Newton, *Kirk-Othmer Encyclopedia of Chemical Technology*, John Wiley & Sons, Inc., 2000.
- 2 D. L. Nelson, A. L. Lehninger and M. M. Cox, *Lehninger principles of biochemistry*, Macmillan, 2008.
- 3 M. Appl, *Ullmann's Encyclopedia of Industrial Chemistry*, Wiley-VCH Verlag GmbH & Co. KGaA, 2000.
- 4 Industrial Efficiency Technology Database, <http://ietd.iipnet.org/content/ammonia>, accessed October 2016.
- 5 R. R. Schrock, *Acc. Chem. Res.*, 2005, **38**, 955–962.
- 6 J. Rittle and J. C. Peters, *J. Am. Chem. Soc.*, 2016, **138**, 4243–4248.
- 7 D. Zhu, L. H. Zhang, R. E. Ruther and R. J. Hamers, *Nat. Mater.*, 2013, **12**, 836–841.
- 8 J. H. Montoya, C. Tsai, A. Vojvodic and J. K. Nørskov, *ChemSusChem*, 2015, **8**, 2180–2186.

- 9 F. Koleli and D. B. Kayan, *J. Electroanal. Chem.*, 2010, **638**, 119–122.
- 10 S. Giddey, S. P. S. Badwal and Kulkarni, *Int. J. Hydrogen Energy*, 2013, **38**, 14576–14594.
- 11 E. Endoh, J. K. Leland and A. J. Bard, *J. Phys. Chem.*, 1986, **90**, 6223–6226.
- 12 S. Licht, B. Cui, B. Wang, F. Li, J. Lau and S. Liu, *Science*, 2014, **345**, 637–640.
- 13 T. Murakami, T. Nishikiori, T. Nohira and Y. Ito, *J. Am. Chem. Soc.*, 2003, **125**, 334–335.
- 14 R. Michalsky, A. Avram, B. Peterson, P. H. Pfromm and A. Peterson, *Chem. Sci.*, 2015, **6**, 3965–3974.
- 15 R. Michalsky, P. H. Pfromm and A. Steinfeld, *Interface Focus*, 2015, **5**, 20140084.
- 16 A. Jain, S. P. Ong, G. Hautier, W. Chen, W. D. Richards, S. Dacek, S. Cholia, D. Gunter, D. Skinner and G. Ceder, *APL Mater.*, 2013, **1**, 011002.
- 17 A. Jain, G. Hautier, S. P. Ong, C. J. Moore, C. C. Fischer, K. A. Persson and G. Ceder, *Phys. Rev. B: Condens. Matter Mater. Phys.*, 2011, **84**, 045115.
- 18 N. Futamura, T. Ichikawa, N. Imanishi, Y. Takeda and O. Yamamoto, Honolulu PRiME Abstract 1137, 2012.
- 19 T. Laude, T. Kobayashi and Y. Sato, *Int. J. Hydrogen Energy*, 2010, **35**, 585–588.
- 20 O. Takeda, M. Li, T. Toma, K. Sugiyama, M. Hoshi and Y. Sato, *J. Electrochem. Soc.*, 2014, **161**, D820–D823.
- 21 M. Chase, *NIST-JANAF Thermochemical Tables*, American Institute of Physics, 4th edn, 1998.
- 22 D. R. Sadoway, *JOM*, 1998, **50**, 24–26.
- 23 E. F. McFarlane and F. C. Tompkins, *Trans. Faraday Soc.*, 1962, **58**, 997–1007.
- 24 P. Chen, Z. Xiong, J. Luo, J. Lin and K. L. Tan, *Nature*, 2002, **420**, 302–304.
- 25 K. Kim, N. Lee, C. Yoo, J. Kim, H. C. Yoon and J. Han, *J. Electrochem. Soc.*, 2016, **163**, F610–F612.
- 26 A. Banerjee, B. D. Yuhas, E. A. Margulies, Y. B. Zhang, Y. Shim, M. R. Wasielewski and M. G. Kanatzidis, *J. Am. Chem. Soc.*, 2015, **137**, 2030–2034.
- 27 R. Lan, J. T. S. Irvine and S. Tao, *Sci. Rep.*, 2013, **3**, 1145.
- 28 M. Radojevic and V. N. Bashkin, *Practical Environmental Analysis*, Royal Society of Chemistry, 2006.
- 29 HITRANonline, <http://hitran.org/>, accessed October 2016.
- 30 C. Addison and B. Davies, *J. Chem. Soc. A*, 1969, 1822–1827.
- 31 H. Wang, W. D. Zhang, Z. Q. Deng and M. C. Chen, *Solid State Ionics*, 2009, **180**, 212–215.
- 32 G. Ertl, *Catal. Rev.*, 1980, **21**, 201–223.
- 33 S. Dahl, A. Logadottir, C. J. H. Jacobsen and J. K. Nørskov, *Appl. Catal., A*, 2001, **222**, 19–29.
- 34 A. Logadottir, T. H. Rod, J. K. Nørskov, B. Hammer, S. Dahl and C. J. H. Jacobsen, *J. Catal.*, 2001, **197**, 229–231.
- 35 O. Hinrichsen, F. Rosowski, A. Hornung, M. Muhler and G. Ertl, *J. Catal.*, 1997, **165**, 33–44.
- 36 X. Zhang, E. A. Davidson, D. L. Mauzerall, T. D. Searchinger, P. Dumas and Y. Shen, *Nature*, 2015, **528**, 51–59.
- 37 J. Tallaksen, F. Bauer, C. Hulteberg, M. Reese and S. Ahlgren, *J. Cleaner Prod.*, 2015, **107**, 626–635.
- 38 J. R. Jennings, *Catalytic ammonia synthesis: fundamentals and practice*, Springer Science & Business Media, 2013.
- 39 P. Tunå, C. Hulteberg and S. Ahlgren, *Environ. Prog. Sustainable Energy*, 2014, **33**, 1290–1297.
- 40 S. Henbest, E. Giannakopoulou, E. Zindler, J. Wu, J. Rooze, J. Chase, D. Hostert and J. V. Houten, *New Energy Outlook 2016*, Bloomberg New Energy Finance, 2016.
- 41 Fertilizer Use and Price, <http://www.ers.usda.gov/data-products/fertilizer-use-and-price.aspx>, accessed October 2016.
- 42 Total Electric Power Industry, U.S. Energy Information Administration, <https://www.eia.gov/electricity/monthly/>, accessed October 2016.
- 43 R. Ehrlich, *Renewable energy: a first course*, CRC Press, 2013.
- 44 D. J. Fray, *JOM*, 2001, **53**, 27–31.
- 45 D. Aurbach, *Nonaqueous electrochemistry*, CRC Press, 1999.
- 46 The Battery Series, <http://www.businessinsider.com/materials-needed-to-fuel-electric-car-boom-2016-10>, accessed June 2017.
- 47 Global Lithium Prices: Benchmark Mineral Intelligence Data, <https://www.theatlas.com/charts/S1Isjut3>, accessed June 2017.
- 48 IGS Inovative Gas Systems: Nitroswing, http://www.igs-italia.com/download_PDF/NS_Series_eng_2011.pdf, accessed June 2017.
- 49 C. C. Addison and B. M. Davies, *J. Chem. Soc. A*, 1969, 1822–1827.
- 50 G. Paolo, B. Stefano, B. Nicola, C. Matteo, C. Roberto, C. Carlo, C. Davide, L. C. Guido, C. Matteo, D. Ismaila, C. Andrea Dal, G. Stefano de, F. Stefano, F. Guido, G. Ralph, G. Uwe, G. Christos, K. Anton, L. Michele, M. Layla, M. Nicola, M. Francesco, M. Riccardo, P. Stefano, P. Alfredo, P. Lorenzo, S. Carlo, S. Sandro, S. Gabriele, P. S. Ari, S. Alexander, U. Paolo and M. W. Renata, *J. Phys.: Condens. Matter*, 2009, **21**, 395502.
- 51 S. R. Bahn and K. W. Jacobsen, *Comput. Sci. Eng.*, 2002, **4**, 56–66.
- 52 J. Wellendorff, K. R. Lundgaard, A. Møgelhøj, V. Petzold, D. D. Landis, J. K. Nørskov, T. Bligaard and K. W. Jacobsen, *Phys. Rev. B: Condens. Matter Mater. Phys.*, 2012, **85**, 235149.